FLAME ACCELERATION AND DEFLAGRATION-TO-DETONATION TRANSITION IN HYDROGEN-OXYGEN MIXTURE IN A CHANNEL WITH TRIANGULAR OBSTACLES

Huahua XIAO*, Xiaoxi LI and Jinhua SUN
State Key Laboratory of Fire Science, University of Science and Technology of China, Hefei, 230027, China, xiaoh@ustc.edu.cn

ABSTRACT

Study of flame acceleration and deflagration-to-detonation transition (DDT) in obstructed channels is an important subject of research for hydrogen safety. Experiments and numerical simulations of DDT in channels equipped with triangular obstacles were conducted in this work. High-speed schlieren photography and pressure records were used to study the flame shape changes, flame propagation, and pressure build up in the experiments. In the simulations, the fully compressible reactive Navier–Stokes equations coupled with a calibrated chemical-diffusion model for stoichiometric hydrogen-oxygen mixture were solved using a high-order numerical method. The simulations were in good agreement with the experiments. The results show that the triangular obstacles significantly promote the flame acceleration and provide conditions for the occurrence of DDT. In the early stages of flame acceleration, vortices are generated in the gaps between adjacent obstacles, which is the main cause for the flame roll-up and distortion. A positive feedback mechanism between the combustion-generated flow and flame propagation results in the variations of the size and velocity of vortices. The flame-vortex interactions cause flame fragmentation and consequently rapid growth in flame surface area, which further lead to flame acceleration. The initially laminar flame then develops into a turbulent flame with the creation of shocks, shock-flame interactions and various flame instabilities. The continuously arranged obstacles interact with shocks and flames and help to create environments in which a detonation can develop. Both flame collision and flame-shock interaction can give rise to detonation in the channels with triangular obstacles.

1.0 INTRODUCTION

The spontaneous acceleration of a flame front is one of the basic manifestations of gaseous combustion and hence the key issue of interest in combustion science and explosion safety [1, 2]. The study of flame acceleration and deflagration-to-detonation transition (DDT) is crucial for the prevention of fire and explosion accidents in confined spaces and the successful operation of detonation-based propulsion applications [3-6]. Prexmied hydrogen and air or oxygen flames have a great propensity to cause DDT, and prevention of DDT is important for hydrogen safety. In addition, promotion of flame acceleration and fruitful usage of the subsequent DDT is also important for the design and operation of rotating detonation engine (RDE) and pulse detonation engines (PDE) [3, 4].

Premixed flame propagating in a channel is actually a highly complicated, dynamic process, involving all of the complexities of ignition, development of a laminar flame, and the subsequent interactions of this flame with boundary layers and pressure wave under changing background conditions [7]. Extensive investigations have been conducted to understand this complex flame acceleration process in a smooth tube [1, 8, 9]. In the process, the flame can undergo various shape changes, such as hemispherical, finger-shaped, tulip, distorted tulip, and cellular flames [10, 11]. The flame eventually propagates at a constant velocity with a range of about 600 m/s to 1000 m/s, which is similar to the sonic speed of the combustion products [12]. In a smooth tube, transition to detonation usually occurs when the flame has accelerated to such velocity [13].

The flame acceleration process inside the channel equipped with obstacles has been of particular interest because these obstacles significantly enhance flame acceleration and more easily trigger detonation compared to the channel with a smooth inner wall [14-17]. Previous studies divided the flame acceleration in the obstructed tube into two main stages [13]. In the first stage, Thermal expansion of combustion products produces flow acceleration in the unburned gas. The obstructions in

the tube distort the unburned gas flow field, resulting in flame area enhancement and the subsequent flame acceleration. Moreover, the interaction of the unburned gas flow with the obstacles forms a vortex downstream of each obstacle that grows in time, eventually forming a recirculation zone between adjacent obstacles. The turbulent combustion in the recirculation zones also leads to additional flame acceleration [13, 16]. In the second phase, compression waves are formed in the unburned gas when the flame speed exceeds the sound speed of the unburned gas. The compression waves then coalesce and eventually form shock waves. The later stage of flame acceleration is governed by shock-flame interactions, which generate flame surface area and further promote turbulent combustion. The shock-flame interactions increase energy release rate [13, 18]. The additional heat release helps to sustain the flame speed and slow the decline in the flame surface [19]. Then the gasdynamic choking due to friction and heat release provides the controlling mechanism for a steady state flame speed close to 1/2 Chapman-Jouguet (CJ) detonation speed [12, 20]. For the more sensitive mixtures, transition to detonation then may occur at the walls.

Deflagration to detonation transition (DDT) is a complex physicochemical phenomenon. The positive feedback phenomenon between combustion and the leading shock wave is the key to flame acceleration and the DDT occurrence, that is, the pressure wave generated by combustion reinforces the leading shock, which in turn further enhances the thermodynamic state of the combustible gas, promoting and accelerating the combustion process. Essentially, the generated detonation wave is a self-ignition wave. Many studies on the characteristics and formation mechanisms of DDT have been conducted using numerical simulations and experiments, and different explanations have been given such as hydrodynamic resistance [18], shock-flame interactions [21], flame folding [19], thermal runaway of fast flames [20], and hot spot initiation. Among them, the hot spot initiation mechanism was first proposed by Zeldovich [21], the hot spot is a region with a reactive gradient, which can be a temperature and/or pressure gradient. In later studies, Lee and Oran et al. [22, 23] confirmed this mechanism through experiments and numerical simulations, respectively. There are many explanations for the hot spot generation, such as turbulent mixing [14], boundary layer effects [22] , shock reflection [18, 19], and shock focusing [4]. Although some possible explanations have been proposed for the formation of DDT, the initiation mechanism has not been fully understood, especially for the formation of DDT under complex geometric conditions. Moreover, it is more difficult to perform accurate simulations to predict the occurrence of the DDT phenomenon.

Many complex geometric conditions are involved in the industrial production process. These obstacles may have different structures and arrangements, which have an important influence on the flame acceleration and DDT in the channels. Most studies have focused on repetitive and spaced plate-like obstacles, cylindrical obstacles or Schelkin spirals in the channel [16, 17, 23]. For plate-like and cylindrical obstacles, the spacing between adjacent obstacles accounts for the pockets with delayed-burning fuel mixture or the recirculation zone, which is crucial for the turbulence and flame acceleration, thus creating conditions for DDT. There is an argument on the role of Shchelkin spiral or some other repeated and continuous obstacles without spacing. Some work showed that the turbulence can also be promoted by the obstacles, thus leading to an enhanced flame acceleration rate then shortening the DDT distance [24]. Valiev et al. [25], however, argued that the triangular obstacles continuously arranged on the channel wall render the flame acceleration slower since it reduces the volume of the fresh gas trapped between the obstacles. The physical mechanism of flame acceleration and DDT in these tubes remains unclear. Among the types of repeated and continuous obstacles, the continuously triangular obstacles can be the representative one. Since this type of geometry is widely used in the surface of industrial transport pipelines and can represent the surface roughness [26, 27]. Nevertheless, the impact of the continuous and triangular obstacles on the flame propagation is not yet clear. The process of flame acceleration and DDT in the obstructed channels with this geometry structure and the mechanism of the process need to be further discussed.

The purpose of this paper is to use experiments and numerical simulations to study the flame acceleration and DDT processes of a highly reactive hydrogen-oxygen gas mixture in a tube with triangular obstacles arranged on the upper and lower walls. High-speed schlieren photography and

pressure measurement were used in the experiments. Numerical simulations are performed by solving the two-dimensional (2D), fully-compressible Navier-Stokes (NS) equations using a high-order numerical method and adaptive mesh refinement (AMR) to simulate the flame acceleration and the subsequent DDT under the same operating conditions as the experiments, to further explore the mechanism of flame acceleration and DDT in the channels equipped with triangular obstacles.

2.0 EXPERIMENTAL SETUP

Fig. 1 shows a schematic of the experimental setup. It is comprised of a constant-volume combustion channel, a high-speed schlieren photography system, a gas mixing device, a high-voltage ignition system, a pressure recording system, and a synchronization controller. The combustion channel is a 300 mm long rectangular duct with a square cross-section of 20 mm × 20 mm. Two quartz glass windows are integrated into the channel front and back sides to facilitate optical access for the visualization of flame acceleration and DDT process. Uniform triangular obstacles are placed continuously along the upper and bottom walls. Each obstacle is 5.8 mm wide and 5 mm high (h). The blockage ratio BR is thus 0.5 (BR = 2h/20). The channel is placed horizontally in the center of the schlieren optical path. The standard Z-configuration schlieren system consists of a point light source, two 300 mm diameter parabolic mirrors, and a high-speed video camera (Photron SAZ 1000K). The images are acquired using a 200 mm lens (f/8) and a band-pass filter (532 +/- 10 nm). In the experiments, the camera is operated at 112500 and 270000 frames per second, respectively.

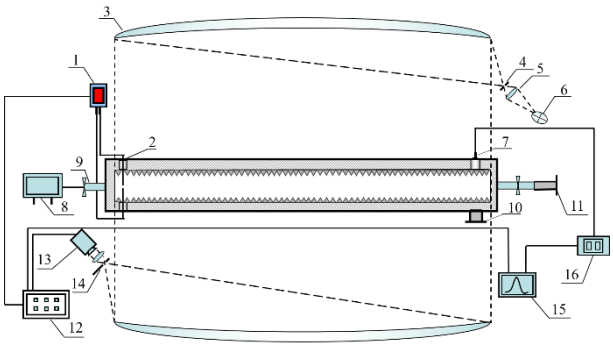

Figure 1. Schematic of the experimental setup: (1) spark igniter, (2) ignition electrode, (3) schlieren mirror, (4) slit, (5) focusing lens, (6) point light source, (7) pressure transducer, (8) gas mixing device, (9) inlet valve, (10) exhaust pipe, (11) discharge vent, (12) synchronization controller, (13) high-speed camera, (14) knife edge, (15) data recorder, (16) charge amplifier

All the experiments are performed using stoichiometric hydrogen-oxygen mixture, which is controlled by the high-precision mass flow meters in the gas mixing device. The initial temperature and pressure are T_0 = 298 K and p_0 = 101.325 kPa, respectively. The pressure recording system consists of a high-frequency dynamic pressure transducer, a charge amplifier and a data recorder. A synchronization controller is used to synchronously control the spark igniter, pressure recorder and high-speed video camera.

3.0 PHYSICAL AND NUMERICAL MODELS

The two-dimensional fully compressible reactive Navier-Stokes (NS) equations are solved using a third-order Godunov algorithm [28]. The combustion of premixed stoichiometric hydrogen and oxygen is modelled by a simplified chemical-diffusive model [29]. The reaction rate is defined as

$$\dot{\omega} = -A\rho Y exp\left(-\frac{E_a}{RT}\right), \quad (1)$$

where A - pre-exponential factor; ρ – density, kg/m^3; Y - reactant mass fraction; E_a - activation energy, kJ/mol; R - universal gas constant; T - temperature, K. The dynamic viscosity μ, mass diffusivity D, and thermal diffusivity k are calculated as a function of temperature:

$$\mu = \mu_0 T^{0.7}/\rho,\ D = D_0 T^{0.7}/\rho,\ k = k_0 T^{0.7}/\rho. \quad (2)$$

The input parameters of the model and the major computed properties of combustion waves for stoichiometric hydrogen-oxygen mixture are given in Table 1. The chemical-diffusive model has been extensively tested and verified by various combustion problems including laminar flames, turbulent flames, cellular detonation, shock-flame interactions and DDT [7, 17, 19, 30].

Table 1. Input model parameters and computed properties for simulating a stoichiometric hydrogen-oxygen mixture

Symbol	Value	Description
Input parameters		
p_0	1.0 atm	Initial pressure
T_0	298 K	Initial temperature
ρ_0	0.61 kg/m^3	Initial density
γ	1.15	Specific heat ratio
M	14.92 g/mol	Molecular weight
A	2.16×10^{13} m^3/kg-s	Pre-exponential factor
E_a	$54.12RT_0$	Activation energy
q	$70.15RT_0/M$	Chemical heat release
$\mu_0 = D_0 = k_0$	3.7×10^{-5} kg/s-m-K$^{0.7}$	Reference coefficients
Laminar flame and Chapman-Jouguet detonation properties		
T_b	3074 K	Adiabatic flame temperature
S_{u0}	9.74 m/s	Laminar burning velocity
δ_L	0.24 mm	Laminar flame thickness
D_{CJ}	2840 m/s	CJ detonation velocity
P_{CJ}	23.56 p_0	Pressure at CJ Point
x_d	0.046 mm	Half-reaction thickness

The numerical setup is the same as described in the experiment. Fig. 2 shows the schematic setup in the simulations. It is a 2 cm high and 30 cm long channel. The obstacle is modelled using an immersed boundary method [31], 5.8 mm wide and 5 mm high. The blockage ratio *BR* of the channel is 0.5. The ignition source is a small circular pocket of burned gas with a radius of 1 mm centred on the channel axis 5.8 mm from the left end wall. Adaptive mesh refinement based on the BoxLib library [32] helps resolve important flow features, such as flames, boundary layers, and pressure waves. Grid resolution tests were conducted by varying the value of the minimum grid sizes. The results show that all the trial grid sizes are adequate for capturing the major features of flame acceleration and detonation transition.

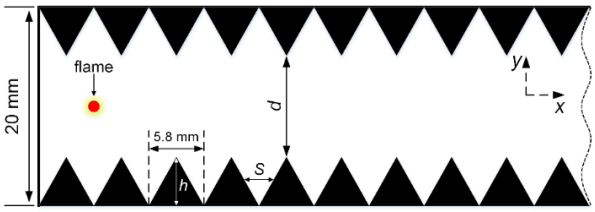

Figure 2. Computational domain of a channel with triangular obstacles. h is the height of the obstacle; d is the unobstructed height of the channel; S is the spacing between middle points of two opposite faces of adjacent obstacles.

4.0 RESULTS AND DISCUSSION

4.1 Flame acceleration in the experiments and numerical simulations

Fig. 3 shows a comparison of experimental and numerical schlieren images at selected times during the premixed flame acceleration at early stages in the channel equipped with triangular obstacles.

Overall, the flame and flow development appear very similar when the flame or the leading shock wave reaches the same position. In the experiments, after ignited by the high-voltage spark, the flame develops into a spherical shape and then expands outward along the radial direction, as shown in Fig. 3a by 0.027 ms. Correspondingly, the flame is ignited by a circular pocket of burned gas in the simulations and enlarges in the similar shape, as shown at 0.026 ms in Fig. 3b. Next, due to the thermal expansion of the combustion products and the confinement of the sidewalls, the flame expands rapidly and is elongated in unobstructed directions along the centerline of the tube [7, 8, 33]. The initially smooth surface of a laminar flame can be wrinkled due to the Darrieus-Landau (DL) instability. This contributes to the growth of flame surface but to a limited extent [34]. Both sides of the flame are becoming curved under the influence of triangular obstacles (see 0.080 ms in Fig. 3a and 0.058 ms in Fig. 3b). Then the flame curvature gradually increases, which rapidly enhances the flame area and further accelerates the combustion.

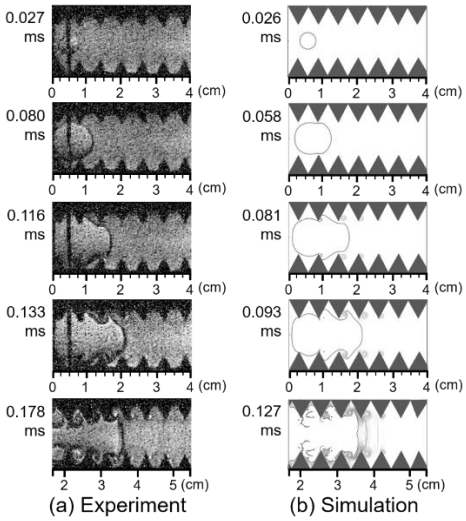

Figure 3. Schlieren images at early stage of flame acceleration in a stoichiometric hydrogen-oxygen mixture in (a) the experiment and (b) the simulation.

When the flame touches the obstacles, acoustic wave is generated in the obstacle gap due to the sudden loss of flame area, which has been providing a source of energy driving flame expansion [35]. The continuous flame surface reduction and the additional heat losses to the sidewalls in the experiments result in the flame deceleration. The interaction of the unburned gas flow with the obstacles forms a pair of vortices between adjacent obstacles that grows in time (e.g., 0.133 ms in Fig. 3a and 0.093 ms in Fig. 3b). These vortices are created in the unburned gas with a circulation that tends to reverse the center part of the flame upstream, thus creating a concaved flame front [7, 36], e.g., 0.178 ms at Fig. 3a and 0.127 ms in Fig. 3b. These vortices control the combustion in the obstacle gap, which causes the flame to accelerate. The flame is entrained into the recirculation zone, stretched and curled by the vortices. As the flame continues to accelerate, the lateral flame is distorted, which increases the flame surface area to a large extent. The speed of the deflagration increases due to the increases in the flame surface area, which, in turn, is caused by flame and vortex interactions. Stronger compression waves are formed in the unburned gas when the flame velocity exceeds the sound speed of the unburned gas at 0.187 ms in Fig. 4a and can be seen more clearly in the simulation results at 0.130 ms in Fig. 4b. The lateral flame wrinkles due to the fluid instabilities caused by the flow acceleration and by interactions of flame-acoustic waves that trigger flow instabilities, for example, Rayleigh–Taylor instability driven by pressure waves [7]. The compression waves then coalesce and eventually form shock waves (e.g., 0.196 ms in Fig. 4a and 0.142 ms in Fig. 4b). The shock waves are then reflected against the upwind surface of the triangular obstacle, resulting in the formation of reflected shock waves. A planar flame front with a cusp pointed towards the burned gas is formed (see 0.204 ms in Fig. 4a and 0.150 ms in Fig. 4b). Then the flame front is gradually distorted from both sides to the middle under the action of shock waves. In the process, the interactions of flame with

shock waves and shear flow produce more flame instabilities, such as the Richtmyer-Meshkov instability (RMI) and the Kelvin-Helmholtz instability (KHI) [21], as shown at 0.150 and 0.168 ms in Fig. 4b. These effects further distort the flame, generate flame surface area and promote turbulent combustion. Multiple flame-shock interactions and merging shocks in unreacted material lead to the development of a strong leading shock wave that moves out in front of the flame front (0.222 ms in Fig. 4a and 0.168 ms in Fig. 4b). As the shock and the flame accelerate, the leading shock remains less than 1 cm ahead of the leading edge of the flame (e.g. 0.168 and 0.197 ms in Fig. 4b). This is the regime of the fast deflagration or fast flame [37]. The leading shock, which diffracts at every obstacle, also reflects from the upwind surface of obstacle after each diffraction. The shock-flame interactions increase the flame surface area and thus the total burning rate [13]. The additional heat release helps to sustain the flame speed and slow the decline in the flame surface. This in turn leads to the increases in the flow velocity and the strength of shock wave [19].

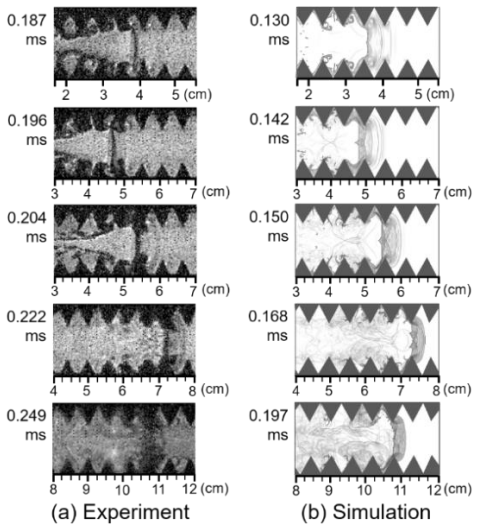

Figure 4. Schlieren images of the premixed hydrogen-oxygen flame front during the premixed flame acceleration at later stage in the channel equipped with triangular obstacles. (a) Experiment; (b) Simulation.

4.2 The DDT process and detonation propagation process

It's difficult to capture the whole process of DDT in the experiment, due to the limitation of shooting speed. However, we can see the moment when the overdriven detonation OD generates from the gap between adjacent obstacles on the upper wall (see, e.g., 0.258 ms in Fig. 5a). The overdriven detonation occurs when conditions behind the leading shock wave (marked with blue dashed curve, and the flame behind is marked in yellow) reach a critical value, and then moves downwards. At the same time, two local detonations generated in the previous gaps propagate towards the centreline of the tube (marked with green arrows at 0.258 ms). The numerical simulations reproduce the similar phenomenon in the experiment, as shown at 0.216 ms in Fig. 5b. The overdriven detonation phase is of very short duration, followed by the phase of stable detonation. At the stage, a unified detonation front is formed, which is marked with red dashed curve at 0.267 ms in Fig. 5a and 0.221 ms in Fig. 5b. The steady detonation propagates at a speed of ~1800 m/s, until it runs out of detonable materials. Strong shock waves form when the detonation front reflects at the upwind surface of the following obstacles (marked with blue arrows at 0.276 ms in Fig. 5a and 0.229 ms in Fig. 5b). The multi-dimensional detonation wave structure, which includes transverse waves and corrugated leading shock wave, can be clearly seen in the schlieren pictures (see, e.g. 0.229 ms in Fig. 5b). Since the simulation is in good agreement with the experiment, we can further discuss the detailed process of DDT using the simulation results.

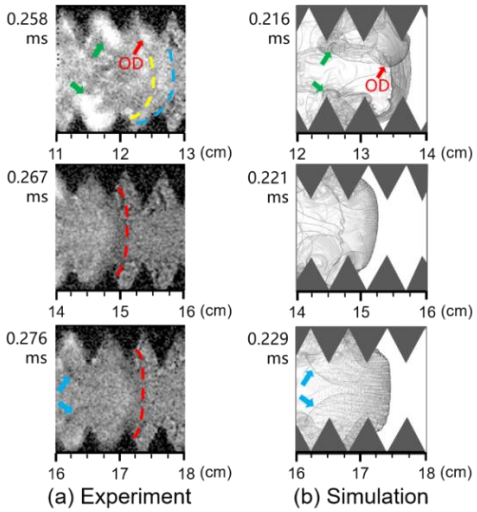

Figure 5. Schlieren fields at the stage of detonation initiation and propagation. (a) Experiment results; (b) Simulation results. OD: overdriven detonation. The green and blue arrows separately indicate the local detonations generated in the previous gap and the strong shock waves form after the stable detonation forms. The yellow, blue and red dashed line indicate the flame, leading shock and detonation front, respectively.

Before the self-sustained overdriven detonation formed, several local detonations occur in the obstacle gap. Fig. 6 shows the temperature fields during the evolution of the first local detonation triggered near the corner between obstacle 16 and 17 starting at about 0.19 ms. As the flame brush propagates towards the corner, a slit of unburned material is created in the cusp between adjacent flame sheets (see 0.1896 ms in Fig. 6). When the flame sheets collide and merge, a local explosion is generated. The explosion spreads outward from the kernel, rapidly burning the unburned gas in the cusps that has been providing an energy source for the maintain of explosion. The explosion wave reaches the flame front at about 0.1897 ms. Then the unburned materials before the flame front are continuously being consumed. A strong detonation (D1) finally formed, supported by the energy provided by the combustion process (see 0.1900 ms).

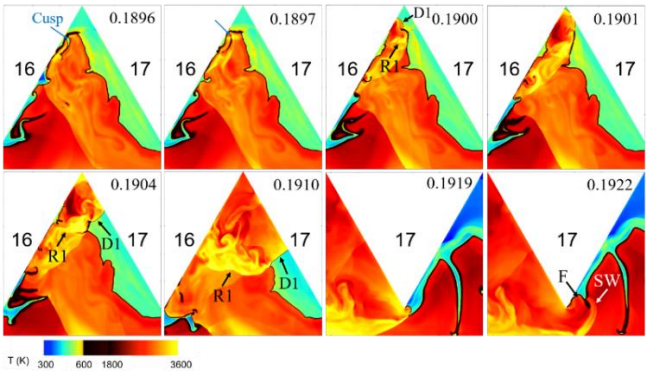

Figure 6. Temperature fields during the evolution of the first local detonation triggered in the gap between obstacle 16 and 17. D1: first local detonation; R1: retonation wave; F: flame; SW: decoupled shock wave. The domain shown in the first six images is from x = 8.99 cm to 9.57 cm and y = 1.4 cm to 2.0 cm, while the last two images is from x = 9.28 cm to 9.86 cm and y = 1.4 cm to 2.0 cm. Time in milliseconds is given in the right-top corner in each frame.

At 0.1900 ms in Fig. 6, the detonation that is formed can be seen propagating towards the bottom of the obstacle gap on the upper wall, and a retonation wave (R1) to the burned area. The detonation is reflected by the upwind surface of obstacle 17 at 0.1901 ms. D1 propagates down the surface of the obstacle 17, consuming the unburned mixture in the gap (0.1904 ms in Fig. 6). R1 travels along the

surface of obstacle 16 at a lower speed compared with D1, thus D1 can gradually catch up with R1 (0.1910 ms). Eventually, D1 and R1 soon unite to one and travels into the remainder of the unburned gas. Then the detonation diffracts over the top of the obstacle 17, as shown at 0.1919 ms. After diffraction, the detonation decays in strength. The reduction in shock strength results in a drop in post shock temperature and a corresponding increase in the chemical induction time [34]. The diffraction is severe enough for the part of the detonation wave near the obstacle tip because of the ~120 °turn, and thus the leading shock wave decouples from the reaction zone (see separate flame F and shock wave SW at 0.1922 ms). The first local detonation does not survive to form a self-sustained detonation.

Next, several local detonations occurred successively in the following gaps between adjacent obstacles. These local detonations usually form after multiple shock reflections and shock-flame interactions and then burn out the unburned gases in the bottom of gap. These detonations themselves do not reach the leading edge of the flame, but generate strong shocks in the burned material, increase the total burning rate, and thus contribute to the strength of the leading shock [15].

At 0.210 ms, flame-shock interactions lead to another detonation D2 at the bottom of obstacle gap near the upper wall (see Fig. 7). Then the detonation propagates along the upwind surface of the obstacle and diffracted through the channel between the top of the triangular obstacle and the flame (see 0.211 ms and 0.212 ms in Fig. 7). The detonation wave consumes the unburned material in the channel and continues to propagate after diffraction (see 0.213 ms). Another detonation D3 occurs near the lower wall, but this detonation is unable to propagate through the very narrow channel (almost no channel) between the obstacle and the flame (see 0.211 and 0.212 ms). Thus D3 fails to propagate after being diffracted (see 0.213 ms). The successfully self-sustained detonation D2 near the upper wall quickly consumes the unburned gas at the bottom of the obstacle gap, reflected on the upwind surface of the next triangular obstacle (at 0.214 ms).

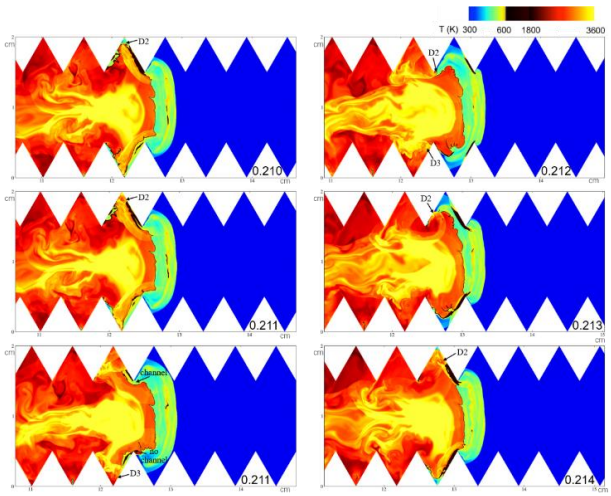

Figure 7. Sequences of temperature maps showing the continuous local detonation occurs in the gaps between adjacent obstacles. D2: second detonation; D3: third detonation. Time in milliseconds is given in the right-bottom corner in each frame.

In the gap between 22nd and 23rd obstacles, the incident shocks are reflected at the upwind surface producing a thick shock layer consisting of multiple superimposed shock waves, as shown at 0.214 ms in Fig. 7. Fig. 8 shows the evolution of the detonation which turns into the final overdriven detonation. In the later stages of flame acceleration, shock-flame interactions are important. At 0.2138 ms, the head-on collisions between reflected shocks and the flame proceed the flame acceleration. An obvious high-temperature protrusion is then generated in front of the main flame surface (see e.g. 0.2139 ms). The protrusion eventually leads to detonation D4 (see Fig. 8 at 0.2140 and 0.2141 ms). The detonation D4 quickly expands and then reflects at the surface of 23rd obstacle (at 0.2142 ms). Flame instabilities arise from shock-flame interactions and a mushroom-shaped detonation develops, as shown at 0.2143

ms. The characteristic expanding mushroom-shaped structures are typical of the Rayleigh-Taylor instabilities and Richtmyer-Meshkov instabilities [38]. The detonation D4 then diffracts at the relatively large gap between the flame and the top of 23rd obstacle, merges with the former detonation D2 at 0.2144 ms. Eventually, an overdriven detonation front (OD) forms (see 0.2148 ms) and then propagates into the unburned region towards the centerline. A larger schlieren field can be seen at 0.216 ms in Fig. 5b.

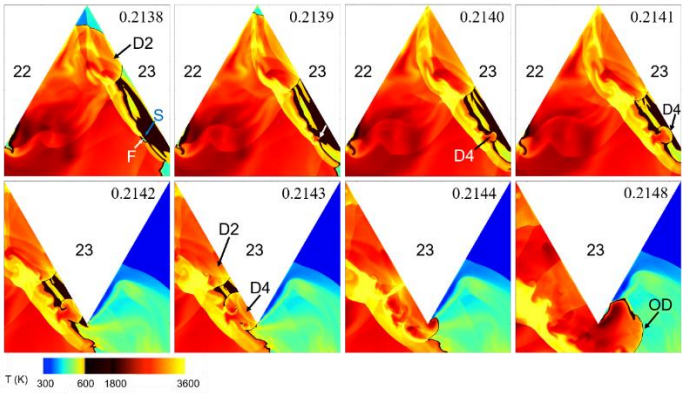

Figure 8. Temperature images showing the detailed generation process of the final overdriven detonation in the gap between obstacle 22 and 23. D2: second detonation; F: flame; S: shock; D4: fourth detonation; OD: overdriven detonation. The white arrow in the image of 0.2139 ms indicates the protrusion generated by flame-shock interactions. The domain shown in the first four images is from x = 8.99 cm to 9.57 cm and y = 1.4 cm to 2.0 cm, while the last four images is from x = 9.28 cm to 9.86 cm and y = 1.4 cm to 2.0 cm. Time in milliseconds is given in the right-top corner.

4.3 Dynamics of the reaction front

Fig. 9 compares reaction-front propagation speed as a function of reaction front position. Fig. 9a compares all the numerical results with the experimental results. In comparison, Fig. 9b compares part of the simulated data with the experimental data at corresponding time points. In the early stages, the flame propagation speed increases due to the flame area production associated with the flame-vortex interactions. Besides, various flow instabilities and the interactions between flame and obstacles contribute to the increases in the flame surface area. The deflagration speed oscillates with a period corresponding to the obstacle spacing. The flame speed in this stage can eventually reach ~450 m/s, which is the sound speed in the unburned mixture.

The large flame velocity oscillations start to appear before 0.05 m in Fig. 9a and 9b. When entering into the fast flame stage, the accelerating turbulent flame generates pressure waves that eventually coalesce into a strong leading shock wave. The flame-shock interaction is responsible for the large flame velocity oscillations observed between 0.05 m and 0.125 m in Fig. 9a and 9b. At the stage, the flame speed may increase to 1480 m/s, that is, about half of the Chapman-Jouguet detonation velocity. The shocks and shock interactions create conditions in which DDT will occur. After several local detonations, the system transitions to a detonation (when the flame reaches about 0.12 m). The detonation is originally overdriven, with a very large wave velocity up to 2962 m/s in experiment 1, 3521 m/s in experiment 2 and 4248 m/s in experiment 3 (see Fig. 9a). The overdriven detonation generated from one side of the channel quickly spreads towards the other side and decays as it propagates. As the overdriven detonation decays to the Chapman–Jouguet (CJ) state, it propagates at a speed of ~ 2840 m/s (both in experiment and simulation), until it runs out of the unburned material.

There are some differences between experimental results and the whole simulation results in Fig. 9a, for example, maximum speed and oscillation frequency. The reason may be that the shooting rate of the high-speed camera in the experiment is much lower than the sampling frequency of the numerical simulation. Thus we change the sampling frequency in the numerical simulations. Simultaneous

simulation results are used for comparison with experiments in Fig. 9b. The simulation results are in good agreement with the experimental results.

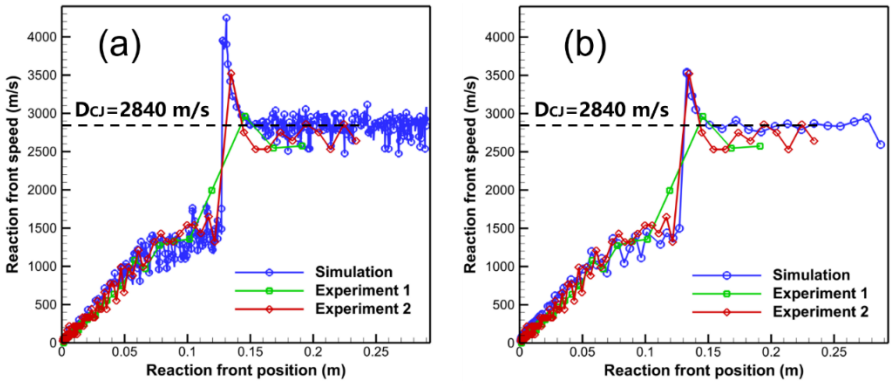

Figure 9. Computed and measured reaction-front propagation speed as a function of reaction front position. (a) Comparison between experiments and simulations using the whole data; (b) Comparison between experiments and simulations using the data for the same moment. The blue line is the simulation result. The green line (Experiment 1) and the red line (Experiment 2) are the results obtained by shooting with a high-speed camera at 112500 and 270000 frames per second, respectively.

5.0 CONCLUSIONS

Experiments and numerical simulations of flame acceleration and DDT in channels continuously equipped with triangular obstacles (BR = 0.5) have been conducted. In the experiments, high-speed schlieren photography and pressure measurement were used to record the flame propagation and DDT process. The high-speed camera was shot at a speed of 112500 and 270000 frames per second, respectively. The simulations solved the two-dimensional, fully compressible reactive Navier-Stokes equations coupled to a single-step Arrhenius chemical-diffusive model for stoichiometric hydrogen-oxygen combustion. The equations were solved using a third-order Godunov algorithm on a dynamically adapting grid. Overall, numerical results are in good agreement with the experimental observations, although they are slightly different in the propagation speed of the reaction front. The simulations well reproduced the flame acceleration and DDT process in the experiments and provided more details of the process through which the flame evolves from a spherical (in experiments) or circular (in simulations) flame, to a distorted flame, to a corrugated flame, to a fast flame, and to the final detonation. Since the experiments were difficult to capture the detailed DDT process due to the limitation of the shooting speed, the numerical results were mainly used in the work to further discuss the mechanism of flame acceleration and DDT.

The early stages of flame acceleration are strongly influenced by the vortices formed within the gaps of adjacent obstacles. Large vortex motion is the main cause of flame roll-up and fragmentation, thus increasing the flame surface area. While small vortices enter the flame structure, enhancing the heat and mass transport. A positive feedback mechanism between the combustion-generated flow and the flame propagation results in the variations of the size and velocity of vortices. The flame-vortex interactions are intensified by the increasing flame velocity, and in turn, maintain the flame acceleration past the triangular obstacles.

The shock-flame interactions play an important role in the later stages of flame acceleration. The interactions between flame and shocks further distort the flame, thus increase flame surface area and promote turbulent combustion through the generated flow instabilities, i.e., Richtmyer-Meshkov instabilities (RMIs) and Kelvin-Helmholtz instabilities (KHIs). The effects are also essential in providing the conditions for multiple local detonations during flame acceleration and the final DDT. The DDT process seems essentially stochastic, and might be related to the fuel, the particular confinement or congestion. What simple need is enough shocks in the system. In the work, the triangular obstacles lead to more frequent and complex shock reflections. A higher flame speed near

the collision point of the shocks is mainly driven by the increasing pressure and temperature of the local gas under the influence of flame-shock interactions. Then the local acceleration of the flame front produces a protrusion. Coherent coupling between chemical reaction and pressure wave results in the transition from the protrusion to detonation. One important result observed in the calculations is that flame collisions can be another reason for detonation initiation in the tube mounted with triangular obstacles. The flame collisions and the following flame merging greatly increase the local temperature and pressure, causing a large flame curvature and an accelerated burning in the cusps. More energy is produced in the process, providing conditions for the spherical detonation.

ACKNOWLEDGEMENTS

This study was supported by the Fundamental Research Funds for the Central Universities (Grant No. WK2320000048) and the National Natural Science Foundation of China (Grant No. 51976210).

REFERENCES

[1] Ciccarelli G, Dorofeev S. Flame acceleration and transition to detonation in ducts. Progress in Energy and Combustion Science. 2008;34:499-550.
[2] Dorofeev SB. Flame acceleration and explosion safety applications. Proceedings of the Combustion Institute. 2011;33:2161-75.
[3] Roy GD, Frolov SM, Borisov AA, Netzer DW. Pulse detonation propulsion: challenges, current status, and future perspective. Progress in Energy and Combustion Science. 2004;30:545-672.
[4] Xiao H, Oran ES. Shock focusing and detonation initiation at a flame front. Combustion and Flame. 2019;203:397-406.
[5] Wolanski P. Detonative propulsion. Proceedings of the Combustion Institute. 2013;34:125-58.
[6] Gray JAT, Lemke M, Reiss J, Paschereit CO, Sesterhenn J, Moeck JP. A compact shock-focusing geometry for detonation initiation: Experiments and adjoint-based variational data assimilation. Combustion and Flame. 2017;183:144-56.
[7] Xiao H, Houim RW, Oran ES. Formation and evolution of distorted tulip flames. Combustion and Flame. 2015;162:4084-101.
[8] Bychkov V, Akkerman Vy, Fru G, Petchenko A, Eriksson L-E. Flame acceleration in the early stages of burning in tubes. Combustion and Flame. 2007;150:263-76.
[9] Valiev DM, Akkerman Vy, Kuznetsov M, Eriksson L-E, Law CK, Bychkov V. Influence of gas compression on flame acceleration in the early stage of burning in tubes. Combustion and Flame. 2013;160:97-111.
[10] Clanet C, Searby G. On the “tulip flame” phenomenon. Combustion and Flame. 1996;105:225-38.
[11] Ponizy B, Claverie A, Veyssière B. Tulip flame - the mechanism of flame front inversion. Combustion and Flame. 2014;161:3051-62.
[12] Lee JH, Knystautas R, Chan CK. Turbulent flame propagation in obstacle-filled tubes. Symposium (International) on Combustion. 1985;20:1663-72.
[13] Ciccarelli G, Johansen CT, Parravani M. The role of shock–flame interactions on flame acceleration in an obstacle laden channel. Combustion and Flame. 2010;157:2125-36.
[14] Oran ES, Gamezo VN. Origins of the deflagration-to-detonation transition in gas-phase combustion. Combustion and Flame. 2007;148:4-47.
[15] Gamezo VN, Ogawa T, Oran ES. Flame acceleration and DDT in channels with obstacles: Effect of obstacle spacing. Combustion and Flame. 2008;155:302-15.
[16] Johansen CT, Ciccarelli G. Visualization of the unburned gas flow field ahead of an accelerating flame in an obstructed square channel. Combustion and Flame. 2009;156:405-16.
[17] Goodwin GB, Houim RW, Oran ES. Effect of decreasing blockage ratio on DDT in small channels with obstacles. Combustion and Flame. 2016;173:16-26.
[18] Gamezo VN, Ogawa T, Oran ES. Numerical simulations of flame propagation and DDT in obstructed channels filled with hydrogen–air mixture. Proceedings of the Combustion Institute. 2007;31:2463-71.

[19] Kessler DA, Gamezo VN, Oran ES. Simulations of flame acceleration and deflagration-to-detonation transitions in methane–air systems. Combustion and Flame. 2010;157:2063-77.
[20] Chue RS, Clarke JF, Lee JH. Chapman-Jouguet deflagrations. Proceedings of the Royal Society of London Series A: Mathematical and Physical Sciences. 1993;441:607-23.
[21] Khokhlov AM, Oran ES, Thomas GO. Numerical simulation of deflagration-to-detonation transition: the role of shock–flame interactions in turbulent flames. Combustion and Flame. 1999;117:323-39.
[22] Houim RW, Ozgen A, Oran ES. The role of spontaneous waves in the deflagration-to-detonation transition in submillimetre channels. Combustion Theory and Modelling. 2016;20:1068-87.
[23] Schelkin KI. Influence of the wall roughness on initiation and propagation of detonation in gases. J Exp Theor Phys. 1940:823.
[24] Asato K, Miyasaka T, Watanabe Y, Tanabashi K. Combined effects of vortex flow and the Shchelkin spiral dimensions on characteristics of deflagration-to-detonation transition. Shock Waves. 2013;23:325-35.
[25] Valiev D, Bychkov V, Akkerman Vy, Law CK, Eriksson L-E. Flame acceleration in channels with obstacles in the deflagration-to-detonation transition. Combustion and Flame. 2010;157:1012-21.
[26] Houim RW, Oran E. Effect of Surface Roughness on Deflagration-to-Detonation Transition in Submilimeter Channels. 26th International Colloquium on the Dynamics of Explosions and Reactive Systems. Boston, MA, USA2017.
[27] Xiao Huahua OES. Flame acceleration and transition to detonation in a channel with triangular obstacles. 27th International Colloquium on the Dynamics of Explosions and Reactive Systems. Beijing, China2019.
[28] Houim RW, Kuo KK. A low-dissipation and time-accurate method for compressible multi-component flow with variable specific heat ratios. Journal of Computational Physics. 2011;230:8527-53.
[29] Kaplan CR, Özgen A, Oran ES. Chemical-diffusive models for flame acceleration and transition-to-detonation: genetic algorithm and optimisation procedure. Combustion Theory and Modelling. 2019;23:67-86.
[30] Poludnenko AY, Gardiner TA, Oran ES. Spontaneous Transition of Turbulent Flames to Detonations in Unconfined Media. Physical Review Letters. 2011;107:054501.
[31] Chaudhuri A, Hadjadj A, Chinnayya A. On the use of immersed boundary methods for shock/obstacle interactions. Journal of Computational Physics. 2011;230:1731-48.
[32] Boxlib. Center for Computational Sciences and Engineering. University of California. Berkeley2015.
[33] Kurdyumov VN, Matalon M. Self-accelerating flames in long narrow open channels. Proceedings of the Combustion Institute. 2015;35:921-8.
[34] Ciccarelli G, Dorofeev S. Flame acceleration and transition to detonation in ducts. Prog Energy Combust Sci. 2008;34:499-550.
[35] Li X, Xiao H, Duan Q, Sun J. Numerical study of premixed flame dynamics in a closed tube: Effect of wall boundary condition. Proceedings of the Combustion Institute. 2020.
[36] Matalon M, Metzener P. The propagation of premixed flames in closed tubes. Journal of Fluid Mechanics. 1997;336:331-50.
[37] Oran ES, Chamberlain G, Pekalski A. Mechanisms and occurrence of detonations in vapor cloud explosions. Progress in Energy and Combustion Science. 2020;77:100804.
[38] Oran ES. Understanding explosions – From catastrophic accidents to creation of the universe. Proceedings of the Combustion Institute. 2015;35:1-35.